

This discussion paper is/has been under review for the journal Atmospheric Chemistry and Physics (ACP). Please refer to the corresponding final paper in ACP if available.

A new method for deriving aerosol solar radiative forcing and its first application within MILAGRO/INTEX-B

K. S. Schmidt¹, P. Pilewskie¹, R. Bergstrom², O. Coddington¹, J. Redemann², J. Livingston³, P. Russell⁴, E. Bierwirth⁵, M. Wendisch⁵, W. Gore⁴, M. K. Dubey⁶, and C. Mazzoleni^{6,7}

¹Laboratory for Atmospheric and Space Physics, Boulder, CO, USA

²Bay Area Environmental Research Institute, Sonoma, CA, USA

³SRI International, Menlo Park, CA, USA

⁴NASA Ames Research Center, Moffett Field, CA, USA

⁵Leipzig Institute for Meteorology, University of Leipzig, Leipzig, Germany

⁶Los Alamos National Laboratory, Los Alamos, NM, USA

⁷Michigan Technological University, MI, USA

Received: 14 January 2010 – Accepted: 23 January 2010 – Published: 3 February 2010

Correspondence to: K. S. Schmidt (sebastian.schmidt@lasp.colorado.edu)

Published by Copernicus Publications on behalf of the European Geosciences Union.

**A new method for
deriving aerosol solar
radiative forcing**

K. S. Schmidt et al.

Title Page

Abstract

Introduction

Conclusions

References

Tables

Figures

◀

▶

◀

▶

Back

Close

Full Screen / Esc

Printer-friendly Version

Interactive Discussion



Abstract

We introduce a method for deriving aerosol spectral radiative forcing, along with single scattering albedo, asymmetry parameter and surface albedo from airborne vertical profile measurements of shortwave spectral irradiance and spectral aerosol optical thickness. The new method complements the traditional, direct measurement of aerosol radiative forcing efficiency from horizontal flight legs below gradients of aerosol optical thickness, and is particularly useful over heterogeneous land surfaces or for homogeneous aerosol layers where the horizontal gradient method is impractical. Using data collected by the Solar Spectral Flux Radiometer (SSFR) and the Ames Airborne Tracking Sunphotometer (AATS-14) during the MILAGRO (Megacity Initiative: Local and Global Research Observations) experiment, we validate an over-ocean spectral aerosol forcing efficiency from the new method by comparing with the traditional method. Retrieved over-land aerosol optical properties are compared with in-situ measurements and AERONET retrievals. The spectral forcing efficiencies over ocean and land are remarkably similar, and agree with results from other field experiments.

1 Introduction

In this paper, we study aerosol radiative properties such as spectral single scattering albedo and asymmetry parameter, as well as spectral radiative forcing during the MILAGRO (Megacity Initiative – Local and Global Research Observations) experiment (Molina et al., 2010). We use irradiance and aerosol optical thickness (AOT) measurements made by the Solar Spectral Flux Radiometer (SSFR, Pilewskie et al., 2003) and the 14-channel Ames Airborne Tracking Sunphotometer (AATS-14, Livingston et al., 2009). These instruments were mounted on the NASA J-31 aircraft (based in Veracruz, Mexico) that conducted 13 research flights over the Gulf of Mexico and the Mexico City area. In previous studies, the combination of irradiance and AOT measurements has been used to derive the so-called aerosol radiative forcing efficiency

A new method for deriving aerosol solar radiative forcing

K. S. Schmidt et al.

Title Page

Abstract

Introduction

Conclusions

References

Tables

Figures

◀

▶

◀

▶

Back

Close

Full Screen / Esc

Printer-friendly Version

Interactive Discussion



**A new method for
deriving aerosol solar
radiative forcing**K. S. Schmidt et al.

[Title Page](#)[Abstract](#)[Introduction](#)[Conclusions](#)[References](#)[Tables](#)[Figures](#)[◀](#)[▶](#)[◀](#)[▶](#)[Back](#)[Close](#)[Full Screen / Esc](#)[Printer-friendly Version](#)[Interactive Discussion](#)

(Pilewskie et al., 2003; Redemann et al., 2006). This quantity describes the change of net irradiance, ΔF , per change of AOT, $\Delta\tau$. Despite the broad spatial and temporal variability inherent in aerosol optical properties, there are some indications that the *relative* spectral forcing efficiency (forcing efficiency normalized by incident irradiance on top of the aerosol layer), is bound within typical ranges. This property makes forcing efficiency a convenient concept to characterize aerosol radiative effects even when little is known about the aerosol microphysical and optical properties, as occurs for example in satellite observations where usually only optical thickness is available.

The traditional method to derive spectral aerosol radiative forcing (hereafter referred to as the gradient method) requires that changes in net irradiance and AOT observed below an aerosol layer are linearly correlated. The forcing efficiency can then be obtained directly from the slope of the regression line. The measurement geometry is illustrated in Fig. 1. Typically, only the bottom of layer (BOL) forcing efficiency is measured for the gradient method. Obtaining TOL forcing efficiency requires an additional flight leg above the layer along the same ground track of the BOL leg. The net irradiance measured above the layer can then be correlated with the AOT measurements from the leg below. The difference between TOL and BOL forcing is equal to the absorption within the aerosol layer; in the same way, it is atmospheric absorption that connects top of atmosphere (TOA) and surface forcing of an atmospheric constituent.

If properties other than AOT (e.g., surface albedo, aerosol single scattering albedo, sun angle) change during the measurement, the gradient method cannot be rigorously applied. In particular, a heterogeneous surface makes the gradient method impractical because changes in net irradiance are caused both by changes in the underlying surface albedo as well as aerosol optical thickness above the leg. Also, the gradient method cannot be applied for homogeneous aerosol layers with negligible gradients in AOT.

Our new method was developed as an alternative approach that can be used over inhomogeneous land surfaces and in case of homogeneous aerosol layers. It has been adapted from a method that was originally developed for deriving aerosol single

scattering albedo from absorption measurements (Bergstrom et al., 2007; Russell et al., 2002). The new method uses spectral irradiance and AOT that are measured in a vertical profile (see Fig. 1). The profile can be flown as a spiral or as a straight ascent or descent (ramp). The aerosol single scattering albedo and asymmetry parameter are derived from the upward, downward, and net spectral irradiance above and below the layer by iteratively adjusting these two values in a radiative transfer model until the modeled irradiance converges to the measured irradiance at flight altitude. The AOT spectrum is required as model input. The retrieved values are then used to calculate the TOL and BOL forcing efficiencies. The new method is not limited to instantaneous forcing efficiencies that are dependent on solar zenith angle: When aerosol single scattering albedo, asymmetry parameter, and surface albedo are known, spectral and broadband forcing efficiencies can be calculated for *any* time and solar zenith angle, or as a diurnally-averaged quantity (Russell et al., 1997).

There are two advantages to this new approach: (1) It does not require a horizontal gradient in AOT since the ascent or descent (ramp or spiral) provides a *vertical* change in AOT and net irradiance even for very homogeneous layers, such as arctic haze events. (2) By restricting a spiral to a radius on the order of a few miles, the impact of variable surface albedo on net irradiance is minimized. There are also disadvantages: (1) Irradiance data from spirals are prone to attitude-correction errors if the optical inlets are not actively stabilized (Wendisch et al., 2001; Bucholtz et al., 2008). This can be partly remedied by flying spirals that have short straight and level sections. (2) Even when limiting the horizontal coverage of the vertical profiles, a horizontal component reflecting variability in the underlying surface or in aerosol parameters may remain; also, the new method requires stability of the aerosol properties during the time of the measurement. (3) Throughout the profile, the footprint (circle from within which half of the signal originates) of the downward looking irradiance sensor increases with altitude, introducing sensitivity to heterogeneous surface and aerosol conditions.

A new method for deriving aerosol solar radiative forcingK. S. Schmidt et al.

[Title Page](#)[Abstract](#)[Introduction](#)[Conclusions](#)[References](#)[Tables](#)[Figures](#)[◀](#)[▶](#)[◀](#)[▶](#)[Back](#)[Close](#)[Full Screen / Esc](#)[Printer-friendly Version](#)[Interactive Discussion](#)

**A new method for
deriving aerosol solar
radiative forcing**K. S. Schmidt et al.

In Sect. 2, we introduce the measurements and methodology of the new method. For one over-ocean case, we compare results for aerosol spectral forcing efficiency with those obtained directly from the gradient method. For one case over land, we show that heterogeneities in land surface albedo prohibit the use of the gradient method, and compare single scattering albedo and asymmetry parameter derived from the new method with in-situ measurements, and with retrievals from Aerosol Robotic Network (AERONET) stations in the Mexico City area. In Sect. 3, we present detailed results, and put them in the context of other measurements. In Sect. 4, we discuss some of the measurements of surface albedo, and its variability (see also Coddington et al., 2008). Section 5 contains discussion of results, conclusions, and future work.

2 Data and methodology

2.1 The MILAGRO experiment

The objectives of the MILAGRO experiment are described by Molina et al. (2010). The J-31 was dedicated to radiometric measurements and remote-sensing of aerosol layers in the Mexico City area (5 flights) and over the Gulf of Mexico (8 flights). Most flight segments described in this paper were conducted under cloud-free conditions. Figure 2 shows the flight tracks of the J-31 on 13 March 2006 (a: case over ocean), and on 19 March 2006 (b: case over land). The flight altitude is color-coded. Within this study, we used two cases over ocean (10 and 13 March 2006), and two cases over land (6 and 19 March 2006). Normal flight patterns included low-altitude runs to characterize AOT gradients. When possible, a high-altitude (above-aerosol) leg along the same ground-track was added for aerosol absorption and TOL forcing efficiency measurements. Over sea, the low-level leg could be flown at 30–40 m a.s.l. Over land, air-traffic control restricted the minimum flight altitude, and the airplane was usually not permitted below 300 m a.g.l. Co-located high- and low-level legs and spirals were flown even over land. On 19 March 2006, the evolution of aerosol optical properties was

[Title Page](#)[Abstract](#)[Introduction](#)[Conclusions](#)[References](#)[Tables](#)[Figures](#)[Back](#)[Close](#)[Full Screen / Esc](#)[Printer-friendly Version](#)[Interactive Discussion](#)

traced from the source (around the ground site T0, Mexico City), to T1 and T2 (regions NE of Mexico City that were affected by urban outflow). In Fig. 2, the labels T0, T1, and T2 denote ground stations where extensive aerosol in-situ observations and limited radiometric measurements were made. In addition to the existing AERONET station in Tamihua (northwest of Veracruz), sun-sky photometers were placed at T0, T1, and T2 for the duration of the field experiment.

2.2 Radiative quantities

2.2.1 Aerosol optical thickness and Ångström parameter

The aerosol optical thickness, τ , is defined as the column-integrated extinction. It is comprised of the aerosol scattering and absorption optical thickness, τ_{sca} and τ_{abs} : $\tau_{\text{tot}} = \tau_{\text{sca}} + \tau_{\text{abs}}$. The ratio between scattering and total optical thickness is the column aerosol single scattering albedo: $\tilde{\omega} = \tau_{\text{sca}} / \tau_{\text{tot}}$. The spectral dependence of the AOT contains information about the particle size distribution. The Ångström parameter, a , describes the decrease of AOT with wavelength λ : $\tau(\lambda) = \tau(\lambda_0) \times (\lambda / \lambda_0)^{-a}$. For small particles, a is large (steep spectral dependence); for large particles, the optical thickness does not strongly depend on wavelength and a is small.

2.2.2 Irradiance and related quantities

Irradiance comprises the radiative energy per unit time and area. The net irradiance, F , (or net flux density) is the difference between downward and upward irradiance, F^\downarrow and F^\uparrow : $F = F^\downarrow - F^\uparrow$. The albedo is the ratio between upward and downward irradiance: $\alpha = F^\uparrow / F^\downarrow$. The layer-absorbed irradiance is obtained from the difference of net irradiance above and below the layer, provided that no radiation escapes horizontally (Chandrasekhar, 1960). This is sometimes referred to as flux divergence, although flux divergence includes horizontal contributions as well. We ignore horizontal heterogeneities and thus horizontal transport of radiation in our one-dimensional approach,

A new method for deriving aerosol solar radiative forcing

K. S. Schmidt et al.

Title Page

Abstract

Introduction

Conclusions

References

Tables

Figures

◀

▶

◀

▶

Back

Close

Full Screen / Esc

Printer-friendly Version

Interactive Discussion



**A new method for
deriving aerosol solar
radiative forcing**K. S. Schmidt et al.

assuming that the studied aerosol layers are homogeneous (which is only an approximation as will be discussed below). In radiative transfer calculations, the Mie scattering phase function is often replaced by the Henyey-Greenstein (HG) phase function that can be represented by a single value, the asymmetry parameter, g . The asymmetry parameter is the first moment of the scattering phase function, and is related to the scattering direction ($g=1$: entirely forward, $g=-1$: entirely backward). For irradiance calculations in air or aerosol layers, the Mie scattering phase function with asymmetry parameter g can often be replaced by the HG phase function with the same g (see, however, Wiscombe and Grams, 1976; Coakley and Chylek, 1975). In such cases the only parameters needed for describing the air or aerosol optical properties are AOT, single scattering albedo and asymmetry parameter.

2.3 Radiometric measurements

For this study, aerosol optical thickness was obtained from AERONET stations and AATS-14. The AERONET sun-sky retrievals (Dubovik et al., 2000) provide wavelength-dependent AOT (and thus Ångström parameter and size information), aerosol single scattering albedo (related to absorption) and asymmetry parameter (which also contains size information). The latter two retrieved quantities are possible for a minimum mid-visible AOT of 0.4 among other conditions. The airborne sunphotometer, AATS-14 (Russell et al., 1999; Livingston et al., 2009), provided total aerosol optical thickness at 14 wavelengths (and thus Ångström parameter). The AATS-14 data were masked for cloud occurrences and corrected for molecular scattering and gas absorption (Livingston et al., 2009). A pre- and post-experiment calibration at Mauna Loa, Hawaii, showed a radiometric stability of better than 0.5% in most channels, translating into AOT uncertainties of 0.002 to 0.006.

The SSFR measured downward and upward spectral irradiance over the spectral range 350–2100 nm, with 8–12 nm spectral resolution. Both optical inlets were fixed-mounted on the aircraft fuselage and connected to the spectrometer system through optical fibers. The wavelength calibration, and the optical inlet correction factor related

[Title Page](#)[Abstract](#)[Introduction](#)[Conclusions](#)[References](#)[Tables](#)[Figures](#)[◀](#)[▶](#)[◀](#)[▶](#)[Back](#)[Close](#)[Full Screen / Esc](#)[Printer-friendly Version](#)[Interactive Discussion](#)

to the incidence angle (so-called cosine-response) were determined in the laboratory prior to the field experiment, and an absolute spectral calibration with a NIST-traceable light source (1000 W lamp) was performed before and after the experiment. The nominal radiometric uncertainty is 3–5% across the spectral range. During the field experiment, the stability of the calibration was monitored with field-calibrators, and the flight-to-flight stability was better than 1%.

The data were corrected for the angular response of the light collectors and for changes in downward irradiance due to aircraft attitude. The attitude correction was necessary because the light collector reference plane (i.e., SSFR horizon) did not always coincide with the actual horizon, due to changes in aircraft pitch, roll, and heading. The correction method (Bannehr and Schwiesow, 1993; Bucholtz et al., 2008) uses the measured attitude angles, offset angles between the aircraft inertial reference system and the optical inlet plane, and the time lag between the GPS time and SSFR time. The maximum angular deviation of the aircraft (and SSFR) attitude with respect to the horizon was limited to 3°. This filter was required because the upward irradiance could not be corrected and because the downward correction is limited to small deviations from horizontal aircraft alignment and cannot account for effects from clouds, the surface, or nearby mountains. The filter was relaxed only if no horizontal sections with low roll angles were encountered (in spiral measurements). The error introduced into irradiance by deviating from horizontal alignment was analyzed by Wendisch et al. (2001) and Bucholtz et al. (2008). For the solar zenith angles encountered, a misalignment of 1° results in 1% uncertainty in downward irradiance. Additional uncertainty is introduced by the angular response of the light collectors which are also affected by horizontal misalignment. This error, as well as the attitude-related error for the upward irradiance, can only be quantified empirically. From spiral measurements, the attitude-related systematic error is estimated to be 3% for the net irradiance.

A new method for deriving aerosol solar radiative forcing

K. S. Schmidt et al.

Title Page

Abstract

Introduction

Conclusions

References

Tables

Figures



Back

Close

Full Screen / Esc

Printer-friendly Version

Interactive Discussion



2.4 Derivation of aerosol solar radiative forcing efficiency

2.4.1 Gradient method

The instantaneous aerosol forcing efficiency (Redemann et al., 2006) is derived from simultaneous changes in aerosol optical thickness at a mid-visible wavelength (499 nm), τ_{499} , and spectral net irradiance, F_λ . Both quantities are linearly correlated and the resulting slope is the spectral forcing efficiency E_λ :

$$E_\lambda = dF_\lambda / d\tau_{499}$$

Note that the forcing efficiency is defined with respect to a mid-visible rather than spectral AOT. The *relative* forcing efficiency: $e_\lambda = E_\lambda / F_\lambda^\downarrow \times 100\%$ (where F_λ^\downarrow is the downwelling irradiance at the top of the layer) can be used to compare aerosol radiative forcing from different experiments since it is fairly independent of aerosol loading (AOT) and, in contrast to E , is also independent of downwelling flux at layer top (which varies with solar zenith angle, time of the year, etc.). Prior to regressing irradiance and optical thickness, the downward irradiance must be corrected for changes in solar zenith angle (SZA; $\mu = \cos(\text{SZA})$). Redemann et al. (2006) use a correction formula from Russell et al. (1999) that requires radiative transfer calculations. Here, we use a more simplistic approach: The corrected irradiance

$$F^\downarrow(\mu_0) = F^\downarrow(\mu) \times (\mu_0 / \mu)$$

is close to the uncorrected irradiance $F^\downarrow(\mu)$ if the time span of the measurement is short, and thus if the range of μ values ($\Delta\mu$) is small; μ_0 is chosen in the center of this range ($\mu_0 \approx \langle \mu \rangle$). Redemann et al. (2006) find that $\Delta\tau > 0.05$ and $\Delta\mu / \Delta\tau \ll 1$ are necessary conditions for the gradient method to work. The latter condition does not hold when a gradient occurs over a long distance or time.

Figure 3 illustrates results using the gradient method for the 13 March 2006, where SSFR net irradiance is plotted versus AATS-14 AOT (both at 499 nm wavelength). Measurements below the aerosol gradient are shown as black open circles. The slope of

A new method for deriving aerosol solar radiative forcing

K. S. Schmidt et al.

Title Page

Abstract

Introduction

Conclusions

References

Tables

Figures

◀

▶

◀

▶

Back

Close

Full Screen / Esc

Printer-friendly Version

Interactive Discussion



the linear regression (black line) represents the BOL forcing efficiency. The closed circles show the TOL measurements that retraced the low-level leg along the same flight track. The AOT values used for the TOL leg were obtained from the closest latitude and longitude along the low-level leg since AATS-14 only measures AOT above the aircraft.

The coordinated legs are denoted flux divergence legs in Fig. 2a. They are delimited by an upward spiral in the east and a downward spiral in the west. TOL and BOL measurements are grouped in two domains (around optical thickness 0.13: eastern part, and 0.27: western part) by a small cumulus cloud that was encountered at 96.6° W. Both irradiance and optical thickness data were screened in order to avoid cloud edge effects. For AATS-14, a cloud flag was created based on the spatial variability of transmission measurements at a resolution nine times higher than the resolution of reported AATS AOT (Redemann et al., 2009). For SSFR, data with increased upward irradiance due to cloud reflection were removed manually for the high and the low level leg. The range of AOT acquired to the west of this cloud (generally higher optical thickness) and to the east (lower optical thickness) were near the limit of $\Delta\tau > 0.05$. Therefore, we combined both domains for the regression. This is not entirely justified: As we will show later (Sect. 3, Figs. 6 and 7), the two areas belong to two different air masses with different single scattering albedo and aerosol asymmetry parameter. When regressing the BOL measurements individually (not shown), different slopes and thus forcing efficiencies are obtained (higher in the western part, and lower in the eastern part). At TOL, near-zero slopes were obtained for the individual domains. The difference between the mean TOL net irradiance in the western and eastern domain (2%) can be attributed to different single scattering albedo values in the two air masses (Fig. 6).

2.4.2 New method

The starting point for the new approach is a pair of irradiance spectra from SSFR: one above ($F_1^\uparrow, F_1^\downarrow$) and one below ($F_0^\uparrow, F_0^\downarrow$) an aerosol layer and its spectral optical thickness τ , which can be obtained from a selected latitude and longitude (denoted X in Fig. 1) along the TOL leg (altitude Z_1) and BOL leg (altitude Z_0) of flux divergence

A new method for deriving aerosol solar radiative forcing

K. S. Schmidt et al.

Title Page

Abstract

Introduction

Conclusions

References

Tables

Figures

◀

▶

◀

▶

Back

Close

Full Screen / Esc

Printer-friendly Version

Interactive Discussion



A new method for deriving aerosol solar radiative forcing

K. S. Schmidt et al.

Title Page

Abstract

Introduction

Conclusions

References

Tables

Figures

◀

▶

◀

▶

Back

Close

Full Screen / Esc

Printer-friendly Version

Interactive Discussion



legs, or from vertical profile measurements. The red symbols in Fig. 3 show attitude corrected net irradiance vs. AOT measurements from a spiral vertical profile near the western end of the flux divergence leg on 13 March 2006. In this case, the slope of the regression (dash-dotted red line) cannot be used to measure forcing efficiency directly because during the profile, changing portions of the aerosol layer are above and below the aircraft. Instead, the regression is used to extrapolate the measurements to $\tau=0.0$ and $\tau=\tau_{\max}$. The attitude-corrected measurements deviate from the regression line by about $\pm 2\%$ which is caused by residuals in the attitude correction that cannot be accounted for. This is the basis for the empirical error given in Sect. 2.3. The linear regression also provides estimates of the uncertainty of the extrapolated irradiance pair: 0.5% in this case. Upward and downward irradiance are extrapolated in the same way.

In the next step, the publicly available radiative transfer model libRadtran (Mayer and Kylling, 2005; www.libradtran.org) with SBDART (Ricchiuzzi, 1998) for atmospheric molecular absorption is used to calculate upward and downward irradiance above and below the layer for the specified wavelength and solar zenith angle. In our case, additional model input such as atmospheric profiles (including relative humidity) was derived from the J-31 meteorological measurements and the extraterrestrial solar irradiance was taken from Kurucz (1992) at 1 nm spectral resolution. Figure 4 shows a flow chart of the algorithm where single scattering albedo, $\bar{\omega}$, asymmetry parameter, g , and surface albedo, α , are iteratively adjusted until the modeled irradiance converges with the measured irradiance:

0 Initialize the model with $\bar{\omega}=0.90$, $g=0.75$ and $\alpha=F_0^\uparrow/F_0^\downarrow$.

1a Run libradtran (loop #1: single scattering albedo $\bar{\omega}$).

1b Compare measured absorbed irradiance $F_{\text{abs},m}=(F_1^\downarrow-F_1^\uparrow)-(F_0^\downarrow-F_0^\uparrow)$ with calculated values $F_{\text{abs},c}$ and determine $\bar{\omega}$ for the next iteration step:

$$\bar{\omega}' = \bar{\omega} \times (F_{\text{abs},c}/F_{\text{abs},m})^{1/10}.$$

A new method for deriving aerosol solar radiative forcing

K. S. Schmidt et al.

Title Page

Abstract

Introduction

Conclusions

References

Tables

Figures

◀

▶

◀

▶

Back

Close

Full Screen / Esc

Printer-friendly Version

Interactive Discussion

1c Repeat steps 1a and 1b until $F_{\text{abs},c} \approx F_{\text{abs},m}$ (within threshold $<0.1\%$).

2a Use the retrieved value for $\bar{\omega}$ from step 1 and run libradtran (loop #2: asymmetry parameter g and surface albedo α). Optionally: Rescale the measured irradiance pairs with factor C such that $F_{1,m}^\downarrow = F_{1,c}^\downarrow$.

5 2b Compare measured and modeled downward irradiance below the layer: $F_{0,m}^\downarrow$ and $F_{0,c}^\downarrow$ and determine g for the next iteration step: $g' = g \times (F_{0,m}^\downarrow / F_{0,c}^\downarrow)^2$.

2c Adjust the surface albedo as follows: $\alpha' = \alpha \times (F_{0,m}^\uparrow / F_{0,m}^\downarrow) / (F_{0,c}^\uparrow / F_{0,c}^\downarrow)$.

2d Repeat steps 2a–c until $F_{0,m}^\downarrow \approx F_{0,c}^\downarrow$ (within threshold $<0.1\%$).

3 Using the reflected upward irradiance rather than the transmitted downward irradiance in step 2, retrieve a second value for the asymmetry parameter, denoted \hat{g} , while leaving the surface albedo and single scattering albedo constant. Use $\hat{g}' = \hat{g} \times (F_{0,c}^\uparrow / F_{0,m}^\uparrow)^2$.

4 Repeat loops 1–3 until the values for $\bar{\omega}$, g , \hat{g} and α are stable.

The exponents in 1b (1/10) and 2b (2) were chosen empirically to optimize convergence speed. They do not impact the result itself. The physical interpretation of g and \hat{g} is identical (first moment of the scattering phase function). Since the asymmetry parameter can be retrieved through transmitted (g , step #2) or reflected irradiance (\hat{g} , step #3), g and \hat{g} are regarded as independent retrievals (although g from #2 is used as initial value for \hat{g} in #3) that are compared afterwards. For a low order scattering atmosphere, g is almost independent of α . The opposite is true for \hat{g} which can only be properly retrieved if the value for α is correct. The difference between g and \hat{g} is a measure of the retrieval consistency. The rescaling in step #2a ensures that the modeled downward irradiance on top of the layer is consistent with the measurements. This is not necessarily the case due to uncertainties in the extraterrestrial irradiance.

A new method for deriving aerosol solar radiative forcing

K. S. Schmidt et al.

Title Page

Abstract

Introduction

Conclusions

References

Tables

Figures

◀

▶

◀

▶

Back

Close

Full Screen / Esc

Printer-friendly Version

Interactive Discussion



Rescaling all four irradiance components is equivalent to rescaling the extraterrestrial irradiance in the model. In this way, the irradiance values are effectively normalized with respect to $F_{1,c}^{\downarrow}$. If the rescale factor C falls outside the 5% range ($0.95 < C < 1.05$), the retrieval failed (for example, due to undetected clouds that were not properly screened out). Furthermore, the retrieval is rejected if the difference between g and \hat{g} is larger than 0.05, or if no convergence was reached after ten iterations.

We found that the single scattering albedo part (step #1) of the algorithm was far less sensitive to model-measurements disagreement in downward TOL irradiance than the asymmetry parameter (similar to Bergstrom et al., 2009). When turning off the rescale factor, C , the results for single scattering albedo were only slightly affected. However, the values for g and \hat{g} differed considerably, and sometimes no convergence was reached.

Figure 5 shows a two-dimensional retrieval plot of g and $\bar{\omega}$, for five SSFR wavelengths (19 March 2006). The two small crosses within each circle represent the retrieved pairs of $\{\bar{\omega}_0, g_0\}$ and $\{\bar{\omega}_0, \hat{g}_0\}$ where the length of the cross bars spans the retrieval range resulting from the uncertainty in AOT. The retrieval range due to the AOT uncertainty, $\Delta\tau$, is simply calculated by running the retrievals with aerosol profiles that correspond to $\tau - \Delta\tau$ and $\tau + \Delta\tau$. At 1558 nm, the retrieval is rejected because the values of g and \hat{g} are 0.05 apart. The circles indicate the boundaries within which

$$\frac{\sqrt{\sum (F_i(\bar{\omega}, g) - F_i(\bar{\omega}_0, g_0))^2}}{F_1^{\downarrow}} < 0.01,$$

where F_i are F_1^{\uparrow} , F_0^{\uparrow} and F_0^{\downarrow} . The large thin error bars reflect the associated range in retrieved single scattering albedo and asymmetry parameter. It should be noted that in the residual formula above, identical weight is given to the three irradiance components. In lieu of a more rigorous error propagation analysis for the new algorithm, we use this root mean square method for testing the sensitivity of the retrievals to the input parameters. Since the irradiance components effectively enter the algorithm relative to

the value of F_1^\downarrow , the absolute radiometric uncertainty is irrelevant for error propagation. The irradiance error is between 0.5% (uncertainty of extrapolated irradiance pairs from spiral measurement, illustrated in Fig. 3) for spiral measurements, and 2% for flux divergence measurements (accuracy of attitude correction). For Fig. 5 and throughout the remainder of this manuscript, we chose 1% accuracy for defining the circle boundaries and error bars.

The shape of the residual plots shows that the single scattering albedo is more constrained than asymmetry parameter. The value of $\bar{\omega}_0$ is only weakly dependent on g_0 . For example, $\bar{\omega}_0$ varies from 0.63 to 0.55 for $g_0=0.57\dots 0.95$ (at 499 nm). In Bergstrom et al. (2001, 2009), only absorbed irradiance is used for the retrieval of $\bar{\omega}_0$, and the result is almost independent of the choice of g . For the new algorithm presented here, the sensitivity to g (although weak) is desired and comes from the separate use of F_1^\downarrow and F_1^\uparrow in the algorithm.

The final values for $\bar{\omega}$, g and α are used to calculate the radiative forcing efficiency. For the spiral in Fig. 3, the solid and dotted red lines represent the calculated net irradiances. Their slopes are the BOL and TOL forcing efficiencies, respectively. The modeled BOL forcing efficiency is similar to its directly measured counterpart (i.e., the slope of the solid red line is similar to that of the black line). The offset between the lines is below 2% which is consistent with the attitude correction errors. The offset is irrelevant for the forcing efficiency which is based on the slope alone.

3 Results

Instantaneous forcing efficiencies are given by the slopes of the solid (BOL) and dotted (TOL) lines in Fig. 3. Table 1 gives a complete overview of forcing efficiencies, single scattering albedo, asymmetry parameter, and surface albedo for 499 nm on 13 and 19 March 2006. From the data around $\tau \approx 0.14$ (eastern flux divergence leg), irradiance spectra from above and below the layer at 96.26° W were chosen, and the iterative

A new method for deriving aerosol solar radiative forcing

K. S. Schmidt et al.

Title Page

Abstract

Introduction

Conclusions

References

Tables

Figures

◀

▶

◀

▶

Back

Close

Full Screen / Esc

Printer-friendly Version

Interactive Discussion



algorithm of the new method was used to retrieve $\bar{\omega}$, g , \hat{g} , and α . Nearby (96.20° W), measurements during a spiral profile were taken. The retrieved values for $\bar{\omega}$ and g , as well as forcing efficiency are nearly identical (Table 1). This shows that the new method provides the same results, regardless of whether the required irradiance pairs below and above the layer are taken from collocated horizontal legs or a vertical profile (Fig. 1). From the measurements around $\tau \approx 0.28$ (western flux divergence leg), a pair of measurements was picked at 97.20° W. A spiral was also flown at 97.20° W, yielding slightly higher results for $\bar{\omega}$.

The BOL relative forcing efficiencies e derived from the spirals and flux divergence legs agree for the eastern and the western leg (about 28%), and are similar to the relative forcing efficiency that was derived directly from the measurements (27%). In contrast, the TOL relative forcing efficiencies differ between the eastern and the western legs (about 5% and 9%). The spiral near the western flux divergence leg gives slightly different results. The directly measured TOL forcing efficiency (0.5%) is unphysical because the two underlying air masses have different properties: The single scattering albedo in the west is 0.90, as opposed to 0.86 (more absorbing) in the east; the asymmetry parameter is 0.68 in the west, as opposed to 0.76 in the east (larger particles).

Since the pairs of irradiance are available along the entire flux divergence leg, the retrievals can be done for each individual point along the leg. Figure 6 shows the single scattering albedo as a function of longitude. It varies from around 0.90 to 0.86 for the western and eastern legs, respectively, which is in close agreement to the results obtained from the two spirals. The AERONET site of Tamihua is further west than shown in the plot and may have been exposed to a different airmass (see Table 1) because it indicated a much less absorbing aerosol. The error in $\bar{\omega}$ (not shown) is composed of the two contributions discussed in Sect. 2.4.2. It increased from ± 0.02 in the west to ± 0.06 in the east. This increase is related to the decreasing optical thickness towards the east: A decreasing AOT generally decreases the sensitivity of the method.

A new method for deriving aerosol solar radiative forcing

K. S. Schmidt et al.

Title Page

Abstract

Introduction

Conclusions

References

Tables

Figures

◀

▶

◀

▶

Back

Close

Full Screen / Esc

Printer-friendly Version

Interactive Discussion



Figure 7 shows the asymmetry parameter for the same leg as in Fig. 6. It increases towards the east, indicating more forward scattering and thus larger particles. A related quantity, the Ångström exponent as derived from the AATS-14 wavelength-dependence of optical thickness, is also shown (red), suggesting a similar trend with respect to the aerosol size distribution. The SSFR-derived asymmetry parameter has an uncertainty of 0.06 in the west and up to 0.15 in the east (not shown), again due to the different AOT. In the east, the uncertainty is as large as the increase in g itself. The highest uncertainty values (0.15) occur below a mid-visible AOT of 0.15, which can be regarded as the lower limit in AOT required for a successful g retrieval.

Figure 8 shows an overview of spectral relative forcing efficiency, single scattering albedo, and asymmetry parameter (from top to bottom), for two cases over ocean (left) and two cases over land (right). AERONET retrievals of $\bar{\omega}$ and g , in-situ measurements of $\bar{\omega}$, and Mie calculations for g are only shown for the land cases. T0, T1, and T2 denote the ground stations in (T0, near the airport) and around (T1, T2) Mexico City (see Fig. 2b for exact locations). The mid-visible wavelength of 499 nm (used in Figs. 3, 6, 7 and Table 1) is marked with a dashed line. For more clarity, error bars are sometimes omitted.

The 19 March case (in right-hand panel) was used to check the consistency of the results from the new method with the direct measurement of forcing efficiency over land. The thick black and yellow lines in Fig. 8b show the BOL relative forcing efficiency as derived from the gradient method. The leg labeled T1/T2 (black line) was located between T1 and T2. It was traced back at higher altitude along an almost identical ground track. Along these collocated flux divergence legs, three irradiance pairs were picked at 19.860° N, 19.885° N, and 19.915° N, and the local forcing efficiencies were calculated via the retrieval of $\bar{\omega}$ and g with the new method. In addition, a spiral near T2 was used (20.01° N). Detailed results for 499 nm are shown in Table 1. While the calculated BOL relative forcing efficiencies are mutually consistent (around 25–35%), the directly measured value in the T1/T2 area is substantially higher (46%). This mismatch is probably due to the gradient in surface albedo (0.11 to 0.13 at 499 nm) that occurred over the

A new method for deriving aerosol solar radiative forcing

K. S. Schmidt et al.

[Title Page](#)[Abstract](#)[Introduction](#)[Conclusions](#)[References](#)[Tables](#)[Figures](#)[◀](#)[▶](#)[◀](#)[▶](#)[Back](#)[Close](#)[Full Screen / Esc](#)[Printer-friendly Version](#)[Interactive Discussion](#)

T1/T2 gradient leg. This 17% change introduces a bias in the regression line, and the slope no longer reflects forcing efficiency alone. For this reason, the gradient method is inappropriate in this case.

The disagreement between directly measured forcing efficiency (i.e., the gradient method) and modeled forcing efficient (i.e. new method) occurs all across the spectrum. In Fig. 8b, the T1/T2 gradient forcing efficiency (thick black line, labeled “BOL T1/T2”) is larger in magnitude than the flux divergence retrieval results north of T1 (thin black line, labeled “~T1”, at 19.885° N), near T2 (blue line, labeled “~T2”, at 19.915° N), and the spiral results at T2 (green line, labeled “T2”, at 20.01° N). Another gradient leg was flown near T0 (yellow line, labeled “BOL T0”), complemented by a descent into the aerosol layer in the same area (grey line, labeled “T0”). In this case, the directly measured forcing efficiency is smaller in magnitude than the modeled values up to a wavelength of 700 nm, and larger above. The cross-over is probably related to the vegetation step (increase of surface albedo over vegetated surfaces at a very near-infrared wavelength). Also, the values of the measured spectrum depend on the choice of the length of the gradient leg. The two factors together are indicative of a bias due to heterogeneous surface albedo.

The spectral single scattering albedo and asymmetry parameter associated with the forcing efficiencies in Fig. 8b are shown in 8d and 8f. For selected cases, the TOL forcing efficiencies were added to Fig. 8b (dotted lines). The extreme BOL forcing efficiency of 65% at 499 nm near T0 can be traced back to an extremely low value of $\bar{\omega} \approx 0.6$ – as opposed to 0.74 to 0.91 for the other sites. Selected ground-based observations are shown in yellow:

- 368 nm: range of $\bar{\omega}$ throughout March 2006 at T1, from Corr et al. (2009)
- 500 nm: Multi-Filter Rotating Shadowband Radiometer (MFRSR) $\bar{\omega}$ retrievals at T1 and T2, from Doran et al. (2009) based on an algorithm by Kassianov et al. (2007)

A new method for deriving aerosol solar radiative forcing

K. S. Schmidt et al.

Title Page

Abstract

Introduction

Conclusions

References

Tables

Figures

◀

▶

◀

▶

Back

Close

Full Screen / Esc

Printer-friendly Version

Interactive Discussion



- 530 nm: in-situ measurements with a nephelometer and a PSAP on 19 March 2006 at T1 and T2, from Doran et al. (2009)
- 532 nm: in-situ measurements on 19 March 2006, from Marley et al. (2009)
- 781 nm: in-situ measurements at T1, measured with the integrated photoacoustic/nephelometer (Arnott et al., 1999) onboard the Aerodyne Mobile Laboratory van at T1. The error bar indicates mean \pm standard deviation; the dotted line extends to the maximum.

Concerning the range of single scattering values, Paredes-Miranda et al. (2009), Doran et al. (2009), and Corr et al. (2009) show that there is a strong diurnal pattern, where minima in $\bar{\omega}$ occur at different times of the day, dependent on the site and altitude, making a direct intercomparison difficult.

The spectral shape of the asymmetry parameter (Fig. 8f) stands out for the spiral at T0 (19 March, in gray). In all other examples, including those above the sea (Fig. 8e) and another spiral over T0 on a different day (6 March, red line), g decreases with wavelength. An *increase* with wavelength is atypical. However, this behavior is not necessarily an artifact, considering that the spiral was flown very near the source(s) of the pollution. Mie calculations show that for spheres with 0.2 μm diameter, the asymmetry parameter does increase up to 500 nm (grey dash-dotted line in Fig. 8f). In contrast, the aerosol particles that prevailed around T0 on the 6 March (red line) appear to be larger: In this case, the spectral shape of g is approximated by Mie calculations for 0.5 μm particles (red dash-dotted line), this time decreasing with wavelength. Summarizing, small (young) particles near the source can cause the observed g spectrum near T0. Also, the single scattering albedo tends to increase by aging, and the low $\bar{\omega}$ value near T0 substantiates the supposition of a young aerosol. Shown in yellow are results from other studies: a range of AERONET-retrieved g (440 nm) at T0 for the entire month (Corr et al., 2009) and a MFRSR-retrieved range of g for five days during March near T0 (Barnard et al., 2008). The AERONET retrievals of g from T0 are shown in black (19 March) and red (6 March).

A new method for deriving aerosol solar radiative forcing

K. S. Schmidt et al.

Title Page

Abstract

Introduction

Conclusions

References

Tables

Figures



Back

Close

Full Screen / Esc

Printer-friendly Version

Interactive Discussion



**A new method for
deriving aerosol solar
radiative forcing**K. S. Schmidt et al.

[Title Page](#)[Abstract](#)[Introduction](#)[Conclusions](#)[References](#)[Tables](#)[Figures](#)[⏪](#)[⏩](#)[◀](#)[▶](#)[Back](#)[Close](#)[Full Screen / Esc](#)[Printer-friendly Version](#)[Interactive Discussion](#)

Generally, due to the limited data set acquired by the J-31, we cannot unambiguously detect an evolution of $\bar{\omega}$ and g from the source(s) downwind to the outflow regions as in Doran et al. (2007). Rather, the measurements on the 19 March and other days occur most likely in areas where the pollution has a variegated origin. For example, as shown in Table 1, the single scattering albedo does increase from south (T0) to north (T2), as expected for the urban outflow air mass, but drops back to lower values in between (e.g., at 19.885° N), probably because younger plumes are intercepted on the way. Under these conditions, it is hard to compare airborne retrievals with ground-based measurements. It is also not surprising that the agreement with AERONET retrievals from the site at T0 for the 6 and 19 March is poor (for single scattering albedo and asymmetry parameter) because of the different sampling volumes and times.

Given the large variability in $\bar{\omega}$ and g , it is surprising that the magnitude and spectral shape of the relative forcing efficiencies are quite similar over ocean (Fig. 8a) and land (Fig. 8b). When excluding T0 measurements, the “campaign-average” relative forcing efficiencies range from –30% at 400 nm to –10% at 1000 nm at BOL, very similar to measurements by Redemann et al. (2006) for INTEX-NA (Intercontinental chemical Transport Experiment – North America). The TOL forcing efficiencies vary between –10% (slightly cooling) and 0% (no radiative effect) across the spectrum. Exceptions are the air masses over ocean that were measured on the eastern part of the flux divergence leg on 13 March, and the one on 10 March, with a value of about –30%. The reason for the deviation from the other cases lies in the single scattering albedo for 10 March, and asymmetry parameter for 13 March (see Fig. 8c and e). Possibly, this different behavior is associated with a humidified aerosol with large particle size. This explanation is supported by the Ångström parameter (Fig. 7) which decreases in magnitude from west to east, along with an increase in asymmetry parameter. Differences between individual forcing efficiency spectra occur mainly in the near-UV. This is mainly caused by the strong UV absorption by black and organic carbon (see Bergstrom et al., 2009).

4 Surface albedo measurements

As discussed earlier, the retrieval of \hat{g} and (to a smaller degree) $\bar{\omega}$ depend on the underlying spectral surface albedo. Also, the forcing efficiency is a function of surface albedo (Russell et al., 2002; Bierwirth et al., 2009). We therefore show some typical surface albedo results from the MILAGRO experiment. Detailed comparisons of along-flight-track surface albedo with satellite-derived values and surface data are given by Coddington et al. (2008). The original correction technique including aerosols was first introduced by Wendisch et al. (2004). The challenge in deriving surface albedo from aircraft or satellite measurements lies in the atmospheric correction where albedo at flight-level is converted into the values at the surface. The correction for the molecular scattering in the layer between the surface and the aircraft is straightforward. However, in the presence of an aerosol layer with unknown optical properties and spatial heterogeneity, the atmospheric correction is increasingly difficult. Further problems arise within atmospheric absorption bands, especially because the concentration of water vapor, the strongest gas absorber in the solar wavelength range, is typically poorly known. In our new approach as described in Sect. 2.4.2, the surface albedo is a “by-product” of the retrieval of $\bar{\omega}$ and g . In Wendisch et al. (2004) and Coddington et al. (2008), these aerosol properties were taken from AERONET retrievals or in-situ measurements. Here, all values are simultaneously retrieved. However, the new method can only be used at locations where pairs of above- and below (or in-) layer measurements of irradiance are available, like in spirals or flux divergence legs. For the retrieval of surface albedo along an entire flight leg at one level such as in Coddington et al. (2008), the new method can therefore not be used.

Figure 9 shows selected results of surface albedo over ocean (a) and land (b). The lines show the spectral surface albedo from the method of Coddington et al. (2008); the points show the results of the new method at some of the AATS-14 wavelengths. The dotted lines in Fig. 9a show the flight level albedo. To test the algorithm of Coddington et al. (2008), data from a high and a low flight leg over the ocean were processed,

A new method for deriving aerosol solar radiative forcing

K. S. Schmidt et al.

Title Page

Abstract

Introduction

Conclusions

References

Tables

Figures

◀

▶

◀

▶

Back

Close

Full Screen / Esc

Printer-friendly Version

Interactive Discussion



resulting in similar sea surface albedo spectra (blue and red lines). The sea surface albedo for 10 March was determined using the new method. The negligible deviation in surface albedo on 13 March can be regarded as a measure of sea surface albedo variability.

5 Over land, the red and black lines show the retrieved surface albedo near T2 and T0 from the method by Coddington et al. (2008), where aerosol properties from AERONET were used for the atmospheric correction. The new method was applied for data from the 19 March 2006, the aforementioned spiral near T2 and the descent near T0 (red and black symbols). For T0, close agreement with the Coddington et al. (2008) results is observed. The results from 6 March west of T0 are also shown (blue symbols). A sensitivity analysis of retrieved surface albedo to aerosol properties (single scattering albedo, asymmetry parameter, and optical thickness) is presented in Coddington et al. (2008). In the T2 area, the surface albedo heterogeneity is larger than around T0. The range is indicated by plotting spectra from the neighborhood of T2
10 (19 March 2006): from an area between T1 and T2 (red symbols), and from a location northwest of T2 (green symbols). The variability is about $\pm 15\%$, which means that the gradient technique for forcing efficiency is not possible in this area, as noted before.

5 Conclusions

We introduced and tested a new method that allows for the simultaneous retrieval of aerosol single scattering albedo $\bar{\omega}$, asymmetry parameter g , surface albedo α , and aerosol forcing efficiencies at the top and bottom of an aerosol layer (TOL and BOL) from airborne aerosol optical thickness and irradiance measurements. This method is useful when a measurement of the forcing efficiency with the gradient method (Redemann et al., 2006) is impractical because (a) the gradient of AOT is too weak, (b)
20 the underlying surface heterogeneity introduces a bias in measured upwelling and net irradiance, (c) the intensive aerosol optical properties ($\bar{\omega}$, g) change during the flight leg, or (d) the solar zenith angle changes too much during the flight leg. In contrast to

A new method for deriving aerosol solar radiative forcing

K. S. Schmidt et al.

Title Page

Abstract

Introduction

Conclusions

References

Tables

Figures

◀

▶

◀

▶

Back

Close

Full Screen / Esc

Printer-friendly Version

Interactive Discussion



the gradient method, the new approach can be used to measure aerosol properties at specific locations provided that pairs of irradiance above and below the layer are available. In this way, measured vertical profiles of irradiance and AOT allow for deriving forcing and aerosol optical properties even if the aerosol is very homogeneous. The spiral measurements minimize the error induced by surface albedo heterogeneity on the local forcing efficiency.

The new method was tested for two cases over land and two cases over ocean. It gave consistent results for single scattering albedo, asymmetry parameter and forcing efficiencies, no matter where the required irradiance pairs were extracted from: vertically stacked legs (flux divergence legs), spirals, or ramps. We also showed that the aerosol single scattering albedo and asymmetry parameter, as retrieved point-by-point along a flux divergence leg over ocean, varied considerably. Both AATS-14 measurements of Ångström exponent and SSFR retrievals of asymmetry parameter revealed the same trends with respect to the size distribution of the sampled aerosol.

Over land, the surface albedo heterogeneity biased the slopes of the regression line between net irradiance and aerosol optical thickness, and thus the gradient method-derived forcing efficiency. This is why the gradient method is traditionally only used over ocean. However, even over ocean, AOT gradient-derived and retrieved BOL and TOL forcing efficiency agreed only marginally within the limits of uncertainty. The reason is that the measurements occurred in two distinct air masses with different aerosol radiative properties, which prohibits using the gradient method where only AOT is allowed to change over some distance. Along-track retrievals of aerosol properties from the new method showed that single scattering albedo and asymmetry parameter were indeed different in each of the air masses.

The results of aerosol optical properties over land were compared with in-situ measurements and retrievals from AERONET and MFRSR. This proved to be challenging because of the extreme heterogeneity of the pollution in the Mexico City area. For example, on a northbound flight leg away from the City Center on 19 March 2006, the single scattering albedo generally increased, as described by Doran et al. (2007)

A new method for deriving aerosol solar radiative forcing

K. S. Schmidt et al.

[Title Page](#)[Abstract](#)[Introduction](#)[Conclusions](#)[References](#)[Tables](#)[Figures](#)[⏪](#)[⏩](#)[◀](#)[▶](#)[Back](#)[Close](#)[Full Screen / Esc](#)[Printer-friendly Version](#)[Interactive Discussion](#)

for aging pollution in MILAGRO. However, it dropped intermittently, probably when encountering a younger plume. Also, the asymmetry parameter did not generally increase further away from the source, as would be expected for growing particle size associated with water uptake in the course of aging. This leads to the conclusion that the flight track intercepted pollution of variegated origin. This heterogeneity might explain the disagreement between our retrievals and AERONET results at T0, for both single scattering albedo and asymmetry parameter. A further complication for direct inter-comparison is the strong diurnal pattern in single scattering albedo (Paredes-Miranda et al., 2009).

The interpretation of spectral single scattering albedo and absorption aerosol optical thickness for MILAGRO is discussed in detail by Bergstrom et al. (2009) who present more cases over ocean and land. In contrast to the new method presented in this study, the Bergstrom algorithm (based on absorbed irradiance only) is not sensitive to (or affected by) the asymmetry parameter. Despite this distinction, the $\bar{\omega}$ retrievals from both algorithms agree within the range of uncertainty. The largest differences occur at near-UV wavelengths, particularly over land where large aerosol absorption occurs.

A further validation for the new algorithm consisted in comparing the ocean surface albedo retrievals (a by-product, in addition to $\bar{\omega}$ and g) to the results using the Codrington et al. (2008) and Wendisch et al. (2004) method where the aerosol properties are prescribed, showing no significant difference. Considerable surface albedo heterogeneity was found in the Mexico City urban region and in its rural surroundings.

The new method encountered problems when the aerosols were too inhomogeneous (for example in spirals where the aircraft intercepted a plume only on one side). For these cases, three-dimensional effects corrupt the retrieval that is based on one-dimensional radiative transfer. Usually, the convergence criteria set for the method was not met for these situations and the two different values for g (from transmitted and reflected irradiance) did not coincide. A further difficulty that affects error analysis is the missing horizontal stabilization of the optical inlets of SSFR which makes both aerosol measurements and error analysis difficult. For future aerosol missions, we are

A new method for deriving aerosol solar radiative forcing

K. S. Schmidt et al.

Title Page

Abstract

Introduction

Conclusions

References

Tables

Figures

◀

▶

◀

▶

Back

Close

Full Screen / Esc

Printer-friendly Version

Interactive Discussion



therefore planning to use stabilized platforms. Furthermore, we will examine three-dimensional effects for both heterogeneous aerosol layers and heterogeneous surface albedo. Since both influence the aerosol forcing efficiency, we are seeking to define an “effective” forcing efficiency that takes these heterogeneous conditions into account.

5 Generally, the spectral relative forcing efficiencies were surprisingly similar for almost all cases during MILAGRO, and to those encountered during INTEX-NA (Redemann et al., 2006): They ranged from –30% at 400 nm to –10% at 1000 nm at BOL, and between –10% and 0% at TOL. Exceptions were measurements in extremely polluted areas near pollution sources and two air masses with large, humidified particles over
10 the Gulf of Mexico. The largest forcing efficiency ranges were encountered at near-UV wavelengths. The remarkable similarity of the observations is in contrast with the expectations, since the forcing efficiency is a function of surface albedo (e.g., Russell et al., 1997, 2002; Bierwirth et al., 2008). More data (for example, from snow-covered surfaces in the Arctic) will be examined to understand this phenomenon.

15 *Acknowledgements.* This work was financed by the NASA atmospheric radiation program (directed by Hal Maring). Sebastian Schmidt and Peter Pilewskie were supported by NASA grant NNX08AI83G, Robert Bergstrom by NNX08AH60. We thank John Pommier and Tony Trias, NASA Ames Research Center, for their technical support before and during the MILAGRO experiment, the crew of the J-31 aircraft, and for the support of the NASA ESPO team in Veracruz, Mexico. We also thank the staff of the AERONET stations in Tamihua (Mexico) and in the Mex-
20 ico City urban area for maintaining the AERONET sites; the T0, T1, and T2 AERONET sites were established specifically for the MILAGRO experiment. The major part of this paper was written while the first author worked at the Meteorological Institute of the University for Natural Resources and Applied Life Sciences in Vienna, Austria. Thanks for the hospitality of P. Weihs,
25 H. Kromp-Kolb and J. Wagner.

A new method for deriving aerosol solar radiative forcing

K. S. Schmidt et al.

[Title Page](#)[Abstract](#)[Introduction](#)[Conclusions](#)[References](#)[Tables](#)[Figures](#)[⏪](#)[⏩](#)[◀](#)[▶](#)[Back](#)[Close](#)[Full Screen / Esc](#)[Printer-friendly Version](#)[Interactive Discussion](#)

References

- Arnott, W. P., Moosmüller, H., Rogers, C. F., Jin, T., and Bruch, R.: Photoacoustic spectrometer for measuring light absorption by aerosols: Instrument description, *Atmos. Environ.*, 33, 2845–2852, 1999.
- 5 Bannehr, L. and Schwiesow, R.: A technique to account for the misalignment of pyranometers installed on aircraft, *J. Atmos. Ocean. Tech.*, 10, 774–777, 1993.
- Barnard, J. C., Volkamer, R., and Kassianov, E. I.: Estimation of the mass absorption cross section of the organic carbon component of aerosols in the Mexico City Metropolitan Area, *Atmos. Chem. Phys.*, 8, 6665–6679, 2008,
10 <http://www.atmos-chem-phys.net/8/6665/2008/>.
- Bergstrom, R. W., Pilewskie, P., Russell, P. B., Redemann, J., Bond, T. C., Quinn, P. K., and Sierau, B.: Spectral absorption properties of atmospheric aerosols, *Atmos. Chem. Phys.*, 7, 5937–5943, 2007,
<http://www.atmos-chem-phys.net/7/5937/2007/>.
- 15 Bergstrom, R. W., Schmidt, K. S., Coddington, O., Pilewskie, P., Guan, H., Livingston, J. M., Redemann, J., and Russell, P. B.: Aerosol spectral absorption in the Mexico City area: results from airborne measurements during MILAGRO/INTEX B, *Atmos. Chem. Phys. Discuss.*, 9, 27543–27569, 2009,
<http://www.atmos-chem-phys-discuss.net/9/27543/2009/>.
- 20 Bucholtz, A., Bluth, R. T., Kelly, B., Taylor, S., Batson, K., Sarto, A. W., Tooman, T. P., and McCoy Jr., R. F.: The Stabilized Radiometer Platform (STRAP) – an actively stabilized horizontally level platform for improved aircraft irradiance measurements, *J. Atmos. Ocean. Tech.*, 25, 2161–2175, doi:10.1175/2008JTECHA1085.1, 2008
- Chandrasekhar, S.: *Radiative Transfer*, Dover Publications Inc., New York, 1960.
- 25 Coakley, J. and Chylek, P.: The two-stream approximation in radiative transfer: Including the angle of the incident radiation, *J. Atmos. Sci.*, 32, 409–418, 1975.
- Corr, C. A., Krotkov, N., Madronich, S., Slusser, J. R., Holben, B., Gao, W., Flynn, J., Lefler, B., and Kreidenweis, S. M.: Retrieval of aerosol single scattering albedo at ultraviolet wavelengths at the T1 site during MILAGRO, *Atmos. Chem. Phys.*, 9, 5813–5827, 2009,
30 <http://www.atmos-chem-phys.net/9/5813/2009/>.

A new method for deriving aerosol solar radiative forcing

K. S. Schmidt et al.

Title Page

Abstract

Introduction

Conclusions

References

Tables

Figures

◀

▶

◀

▶

Back

Close

Full Screen / Esc

Printer-friendly Version

Interactive Discussion



**A new method for
deriving aerosol solar
radiative forcing**K. S. Schmidt et al.

[Title Page](#)[Abstract](#)[Introduction](#)[Conclusions](#)[References](#)[Tables](#)[Figures](#)[◀](#)[▶](#)[◀](#)[▶](#)[Back](#)[Close](#)[Full Screen / Esc](#)[Printer-friendly Version](#)[Interactive Discussion](#)

Doran, J. C., Barnard, J. C., Arnott, W. P., Cary, R., Coulter, R., Fast, J. D., Kassianov, E. I., Kleinman, L., Laulainen, N. S., Martin, T., Paredes-Miranda, G., Pekour, M. S., Shaw, W. J., Smith, D. F., Springston, S. R., and Yu, X.-Y.: The T1-T2 study: evolution of aerosol properties downwind of Mexico City, *Atmos. Chem. Phys.*, 7, 1585–1598, 2007,

<http://www.atmos-chem-phys.net/7/1585/2007/>.

Dubovik, O., Smirnov, A., Holben, B. N., King, M. D., Kaufman, Y. J., Eck, T. F., and Slutsker, I.: Accuracy assessments of aerosol optical properties retrieved from Aerosol Robotic Network (AERONET) Sun and sky radiance measurements, *J. Geophys. Res.*, 105(D8), 9791–9806, 2000.

Kassianov, E. I., Flynn, C. J., Ackerman, T. P., and Barnard, J. C.: Aerosol single-scattering albedo and asymmetry parameter from MFRSR observations during the ARM Aerosol IOP 2003, *Atmos. Chem. Phys.*, 7, 3341–3351, 2007,

<http://www.atmos-chem-phys.net/7/3341/2007/>.

Livingston, J. M., Redemann, J., Russell, P. B., Torres, O., Veihelmann, B., Veefkind, P., Braak, R., Smirnov, A., Remer, L., Bergstrom, R. W., Coddington, O., Schmidt, K. S., Pilewskie, P., Johnson, R., and Zhang, Q.: Comparison of aerosol optical depths from the Ozone Monitoring Instrument (OMI) on Aura with results from airborne sunphotometry, other space and ground measurements during MILAGRO/INTEX-B, *Atmos. Chem. Phys.*, 9, 6743–6765, 2009,

<http://www.atmos-chem-phys.net/9/6743/2009/>.

Marley, N. A., Gaffney, J. S., Castro, T., Salcido, A., and Frederick, J.: Measurements of aerosol absorption and scattering in the Mexico City Metropolitan Area during the MILAGRO field campaign: a comparison of results from the T0 and T1 sites, *Atmos. Chem. Phys.*, 9, 189–206, 2009,

<http://www.atmos-chem-phys.net/9/189/2009/>.

Molina, L. et al.: An overview of the MILAGRO 2006 campaign: Mexico City emissions and their transport and transformation, *Atmos. Chem. Phys.*, to be submitted, 2010.

Paredes-Miranda, G., Arnott, W. P., Jimenez, J. L., Aiken, A. C., Gaffney, J. S., and Marley, N. A.: Primary and secondary contributions to aerosol light scattering and absorption in Mexico City during the MILAGRO 2006 campaign, *Atmos. Chem. Phys.*, 9, 3721–3730, 2009,

<http://www.atmos-chem-phys.net/9/3721/2009/>.

**A new method for
deriving aerosol solar
radiative forcing**K. S. Schmidt et al.

- Pilewskie, P., Pommier, J., Bergstrom, R., Gore, W., Howard, S., Rabbette, M., Schmid, B., Hobbs, P. V., and Tsay, S. C.: Solar spectral radiative forcing during the Southern African Regional Science Initiative, *J. Geophys. Res.*, 108(D13), 8486, doi:10.1029/2002JD002411, 2003.
- 5 Redemann, J., Pilewskie, P., Russell, P. B., Livingston, J. M., Howard, S., Schmid, B., Pommier, J., Gore, W., Eilers, J., and Wendisch, M.: Airborne measurements of spectral direct aerosol radiative forcing in the intercontinental chemical transport experiment/intercontinental transport and chemical transformation of anthropogenic pollution, 2004, *J. Geophys. Res.*, 111, D14210, doi:10.1029/2005JD006812, 2006.
- 10 Russell, P. B., Kinne, S., and Bergstrom, R.: Aerosol climate effects: local radiative forcing and column closure experiments, *J. Geophys. Res.*, 102, 9397–9407, 1997.
- Russell, P. B., Livingston, J. M., Hignett, P., Kinne, S., Wong, J., and Hobbs, P. V.: Aerosol-induced radiative flux changes off the United States Mid-Atlantic coast: comparison of values calculated from sunphotometer and in situ data with those measured by airborne pyranometer, *J. Geophys. Res.*, 104, 2289–2307, 1999.
- 15 Russell, P. B., Redemann, J., Schmid, B., Bergstrom, R. W., Livingston, J. M., McIntosh, D. M., Hartley, S., Hobbs, P. V., Quinn, P. K., Carrico, C. M., Rood, M. J., Öström, E., Noone, K. J., von Hoyningen-Huene, W., and Remer, L.: Comparison of aerosol single scattering albedos derived by diverse techniques in two North Atlantic experiments, *J. Atmos. Sci.*, 59, 609–619, 2002.
- 20 Wendisch, M., Müller, D., Schell, D., and Heintzenberg, J.: An airborne spectral albedometer with active horizontal stabilization, *J. Atmos. Ocean. Tech.*, 18, 1856–1866, 2001.
- Wendisch, M., Pilewskie, P., Jäkel, E., Schmidt, S., Pommier, J., Howard, S., Jonsson, H. H., Guan, H., Schröder, M., and Mayer, B.: Airborne measurements of areal spectral surface albedo over different sea and land surfaces, *J. Geophys. Res.*, 109, D08203, doi:10.1029/2003JD004392, 2004.
- 25 Wiscombe, W. J. and Grams, G. W.: The backscattered fraction in two-stream approximations, *J. Atmos. Sci.*, 33, 2440–2451, 1976.

[Title Page](#)[Abstract](#)[Introduction](#)[Conclusions](#)[References](#)[Tables](#)[Figures](#)[◀](#)[▶](#)[◀](#)[▶](#)[Back](#)[Close](#)[Full Screen / Esc](#)[Printer-friendly Version](#)[Interactive Discussion](#)

Table 1. Aerosol optical properties and BOL/TOL forcing efficiencies from SSFR direct measurements, measurement/model approach, and AERONET retrievals, for the case on 13 and 19 March (over ocean and over land). All results for 499 nm wavelength. The AERONET forcing efficiencies are calculated based on the optical properties ($\bar{\omega}$ and g), and on the prevailing surface albedo value α in the area. No $\bar{\omega}$ and g values were retrieved from the direct forcing measurements (gradient legs). From the AERONET retrievals, forcing efficiencies were calculated (italic values). For the land case, measurements are arranged from south to north (increasing distance from the source) going down the table.

20060313 (“ocean”)	optical properties	E ($\text{W m}^{-2} \text{ nm}^{-1} / \tau_{499}$)		e ($\% / \tau_{499}$)	
		BOL	TOL	BOL	TOL
96.26° W flux divergence	$\bar{\omega}=0.862, g=0.74$	-0.402	-0.093	-31.0	-6.3
96.20° W spiral	$\bar{\omega}=0.863, g=0.78$	-0.363	-0.062	-28.0	-4.2
97.20° W flux divergence	$\bar{\omega}=0.898, g=0.68$	-0.366	-0.132	-28.2	-9.0
97.20° W spiral	$\bar{\omega}=0.907, g=0.67$	-0.322	-0.083	-24.8	-6.4
gradient measurement	n.a.	-0.349	-0.006	-26.9	-0.5
Tamihua AERONET	$\bar{\omega}=0.993, g=0.72$	<i>-0.188</i>	<i>-0.172</i>	<i>-13.9</i>	<i>-11.7</i>
20060319 (“land”)					
T0 19.48° N ramp	$\bar{\omega}=0.610, g=0.76, \alpha=0.11$	-0.918	-0.253	-65.2	-16.1
T0 gradient measurement	n.a.	-0.629	n.a.	-43.1	n.a.
T0 AERONET, 19.48° N	$\bar{\omega}=0.747, g=0.76$	<i>-0.630</i>	<i>0.056</i>	<i>-43.8</i>	<i>3.3</i>
19.860° N flux divergence	$\bar{\omega}=0.871, g=0.67, \alpha=0.13$	-0.360	-0.054	-24.8	-3.4
19.885° N flux div. (~T1)	$\bar{\omega}=0.839, g=0.60, \alpha=0.12$	-0.457	-0.080	-27.4	-5.1
19.915° N flux div. (~T2)	$\bar{\omega}=0.878, g=0.59, \alpha=0.11$	-0.384	-0.105	-24.9	-6.6
T2 20.01° N spiral	$\bar{\omega}=0.917, g=0.72, \alpha=0.08$	-0.530	-0.157	-33.0	-9.5
T1/T2 gradient meas.	19.86–19.94° N	-0.649	-0.172	-46.1	-11.8

A new method for deriving aerosol solar radiative forcing

K. S. Schmidt et al.

Title Page

Abstract

Introduction

Conclusions

References

Tables

Figures

◀

▶

◀

▶

Back

Close

Full Screen / Esc

Printer-friendly Version

Interactive Discussion



A new method for deriving aerosol solar radiative forcing

K. S. Schmidt et al.

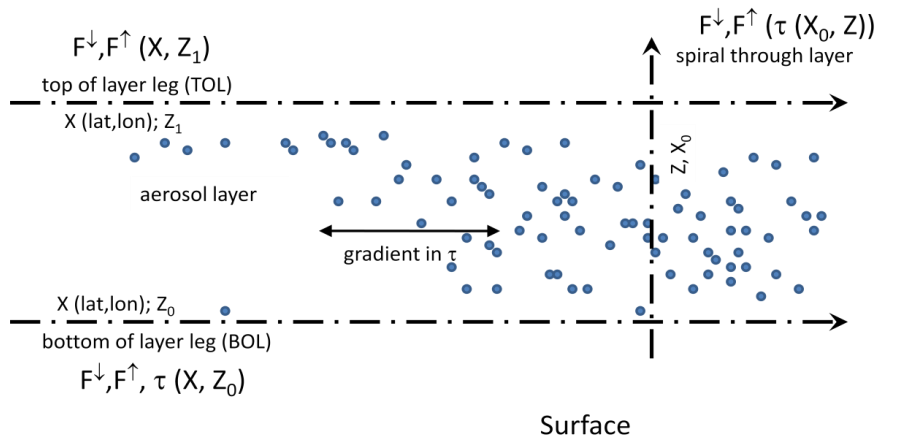


Fig. 1. A horizontal flight leg below an aerosol gradient can be used to measure aerosol bottom of layer (BOL) forcing efficiency directly. An additional leg above the layer that traces back the leg below provides the layer absorption and top of layer (TOL) forcing efficiency. The vertical profile is exploited by the new method.

Title Page

Abstract

Introduction

Conclusions

References

Tables

Figures

◀

▶

◀

▶

Back

Close

Full Screen / Esc

Printer-friendly Version

Interactive Discussion



A new method for deriving aerosol solar radiative forcing

K. S. Schmidt et al.

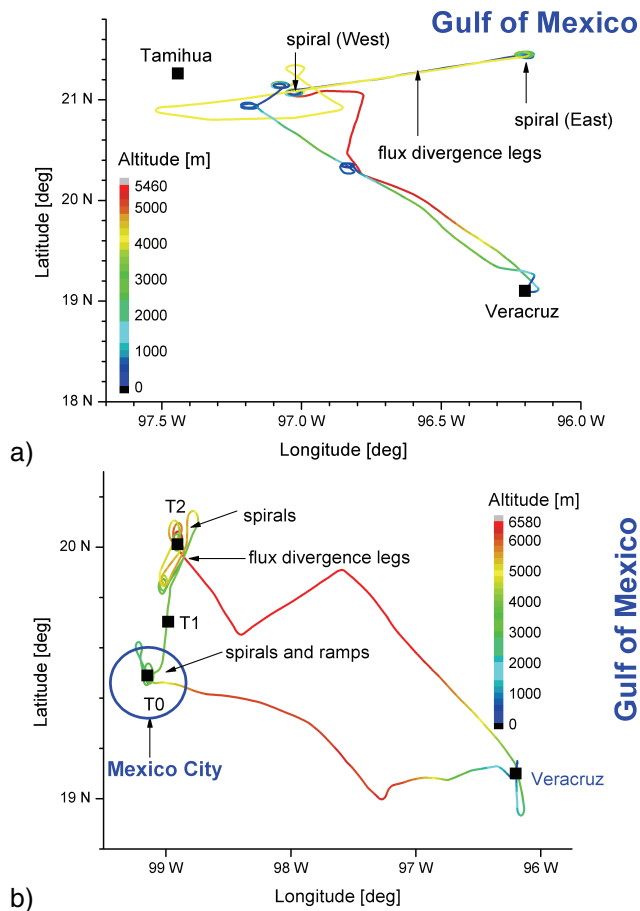


Fig. 2. Flight tracks of the NASA J-31 aircraft on 13 March **(a)** and 19 March 2006 **(b)**, color-coded for flight altitude. T0, T1, and T2 are ground sites of the experiment that were equipped with sun-sky photometers. Tamihua is a permanent AERONET site.

Title Page

Abstract

Introduction

Conclusions

References

Tables

Figures

◀

▶

◀

▶

Back

Close

Full Screen / Esc

Printer-friendly Version

Interactive Discussion



A new method for deriving aerosol solar radiative forcing

K. S. Schmidt et al.

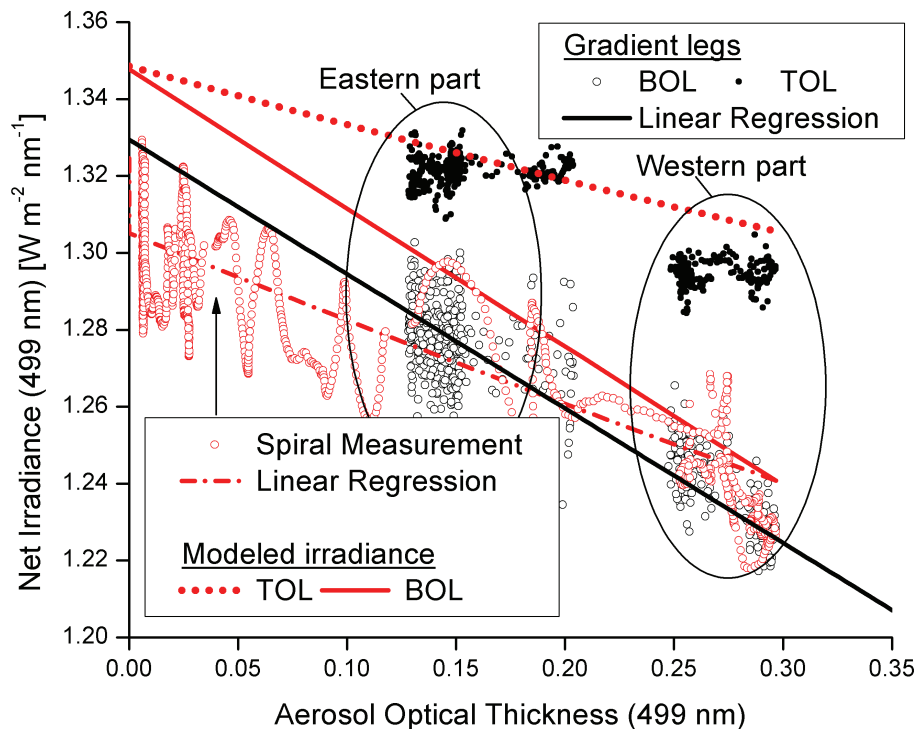


Fig. 3. Net irradiance (499 nm) versus AOT (499 nm), for 13 March 2006 (case over ocean). Black symbols and lines illustrate the gradient method: Measurements below the aerosol gradient (BOL) are shown as open circles and closed circles above (TOL); the regression line is derived from data of both portions of a leg (Western and Eastern part) that is separated by a dissipating cloud in the middle. Spiral profile measurements are shown as red circles. The regression line (red dash-dotted line) is used to extrapolate irradiance pairs above and below the aerosol layer. These pairs are used in the iterative method to retrieve aerosol single scattering albedo and asymmetry parameter. The derived BOL and TOL forcing efficiencies are shown as slopes of the solid and dotted red lines.

Title Page

Abstract

Introduction

Conclusions

References

Tables

Figures

◀

▶

◀

▶

Back

Close

Full Screen / Esc

Printer-friendly Version

Interactive Discussion



A new method for deriving aerosol solar radiative forcing

K. S. Schmidt et al.

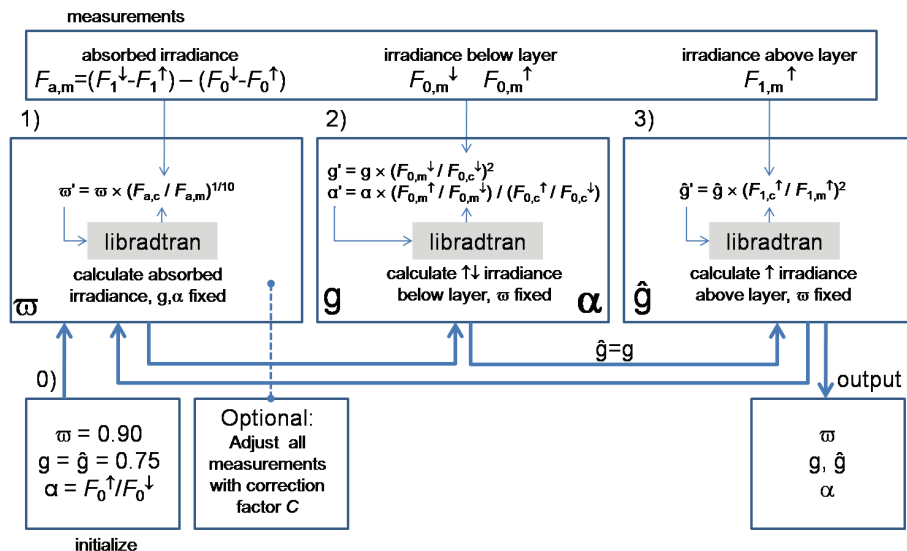


Fig. 4. Flow chart of the iterative algorithm for the retrieval of single scattering albedo, $\bar{\omega}$, asymmetry parameter, g and \hat{g} , and surface albedo, α , from the input irradiance pairs and the optical thickness with the libradtran radiative transfer model.

Title Page

Abstract

Introduction

Conclusions

References

Tables

Figures

◀

▶

◀

▶

Back

Close

Full Screen / Esc

Printer-friendly Version

Interactive Discussion



A new method for deriving aerosol solar radiative forcing

K. S. Schmidt et al.

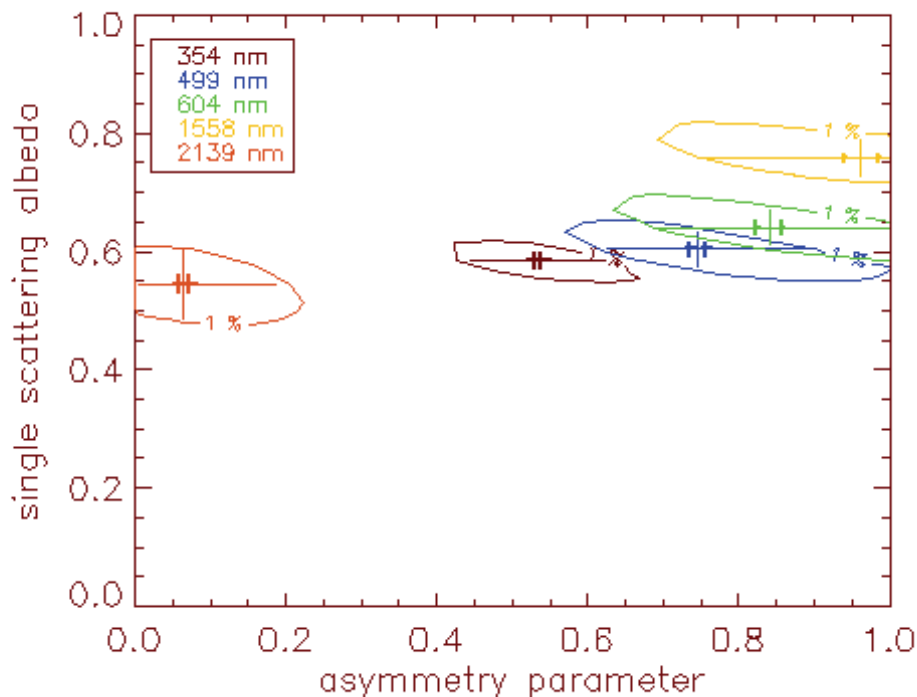


Fig. 5. Two-dimensional retrieval plot of asymmetry parameter g and \hat{g} , and single scattering albedo $\bar{\omega}$, for five SSFR wavelengths (19 March 2006). The two small crosses within each circle represent the retrieved pairs of $\{\bar{\omega}_0, g_0\}$ and $\{\bar{\omega}_0, \hat{g}_0\}$ where the length of the bars spans the retrieval range that is introduced by the uncertainty in AOT. The circles indicate the boundaries within which the root mean square of $F_i(\bar{\omega}, g) - F_i(\bar{\omega}_0, g_0)$ is below 1% of F_1^\dagger , where F_i are F_1^\dagger , F_0^\dagger and F_0^\ddagger ; the large thin error bars reflect the associated range in retrieved single scattering albedo and asymmetry parameter.

Title Page

Abstract

Introduction

Conclusions

References

Tables

Figures

◀

▶

◀

▶

Back

Close

Full Screen / Esc

Printer-friendly Version

Interactive Discussion



**A new method for
deriving aerosol solar
radiative forcing**

K. S. Schmidt et al.

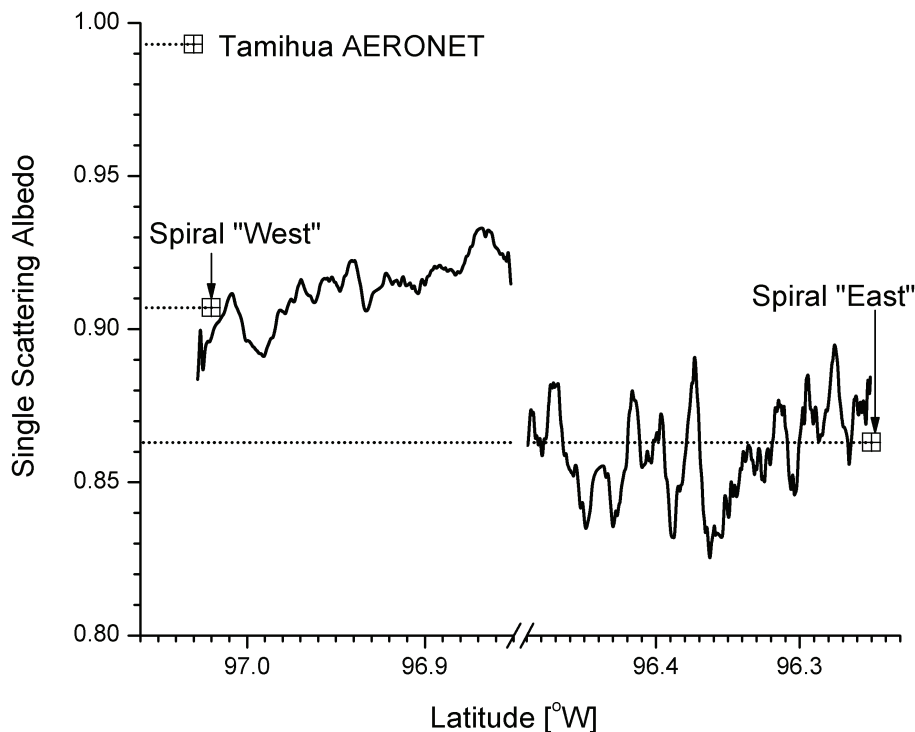


Fig. 6. Single scattering albedo (499 nm) for the flux divergence leg from the case over sea (13 March 2006). The AERONET retrieval comes from the AERONET station of Tamihua that is located west of the flux divergence leg near the coastline.

[Title Page](#)[Abstract](#)[Introduction](#)[Conclusions](#)[References](#)[Tables](#)[Figures](#)[◀](#)[▶](#)[◀](#)[▶](#)[Back](#)[Close](#)[Full Screen / Esc](#)[Printer-friendly Version](#)[Interactive Discussion](#)

**A new method for
deriving aerosol solar
radiative forcing**

K. S. Schmidt et al.

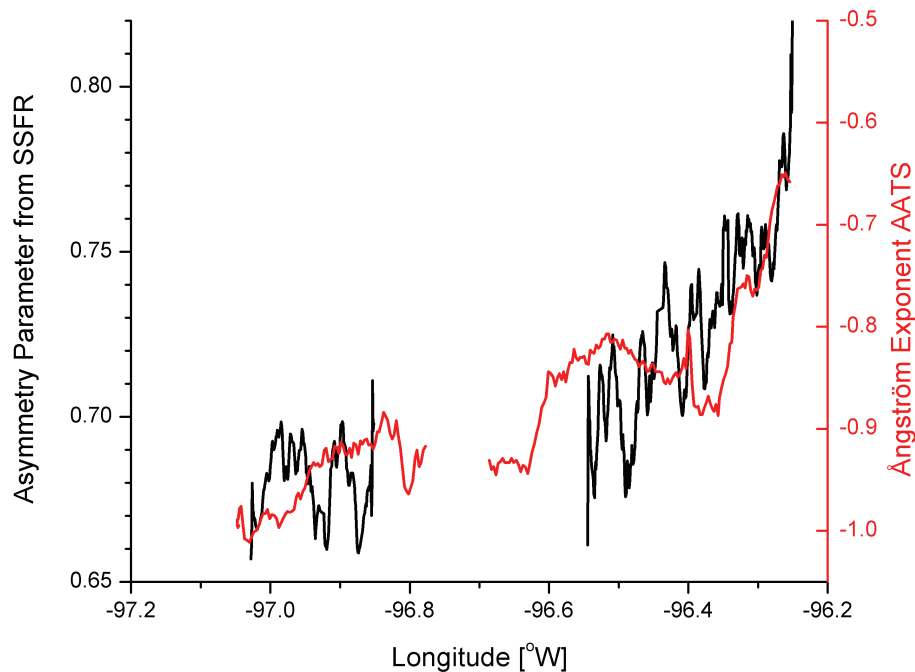


Fig. 7. Asymmetry parameter (black) from SSFR and Ångström exponent (red) from AATS-14 for the same case as Fig. 6, both at 499 nm.

[Title Page](#)[Abstract](#)[Introduction](#)[Conclusions](#)[References](#)[Tables](#)[Figures](#)[◀](#)[▶](#)[◀](#)[▶](#)[Back](#)[Close](#)[Full Screen / Esc](#)[Printer-friendly Version](#)[Interactive Discussion](#)

A new method for deriving aerosol solar radiative forcing

K. S. Schmidt et al.

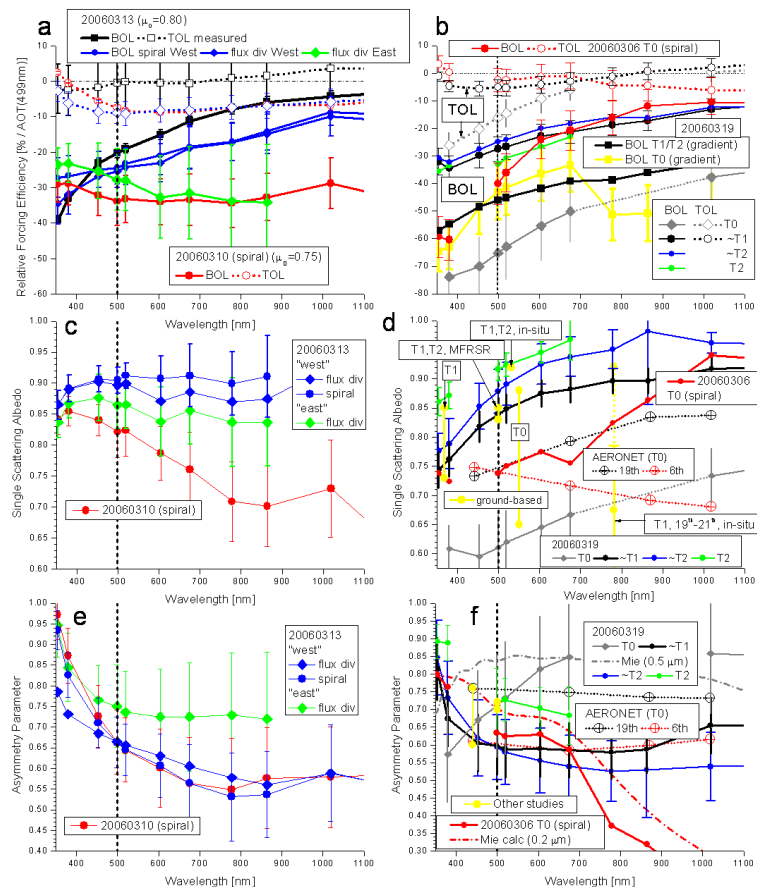


Fig. 8. Overview of spectral forcing efficiency, single scattering albedo, and asymmetry parameter (from top to bottom), over ocean (left: 10 and 13 March 2006) and over land (right: 6 and 19 March 2006). AERONET retrievals, in-situ measurements (of single scattering albedo), and Mie calculations (for asymmetry parameter) are only shown for the land cases. T0, T1, and T2 denote the ground stations in (T0) and around Mexico City. The mid-visible wavelength of 499 nm (used in Figs. 3, 6, 7 and Table 1) is marked with a dashed line.

Title Page

Abstract

Introduction

Conclusions

References

Tables

Figures

◀

▶

◀

▶

Back

Close

Full Screen / Esc

Printer-friendly Version

Interactive Discussion



**A new method for
deriving aerosol solar
radiative forcing**

K. S. Schmidt et al.

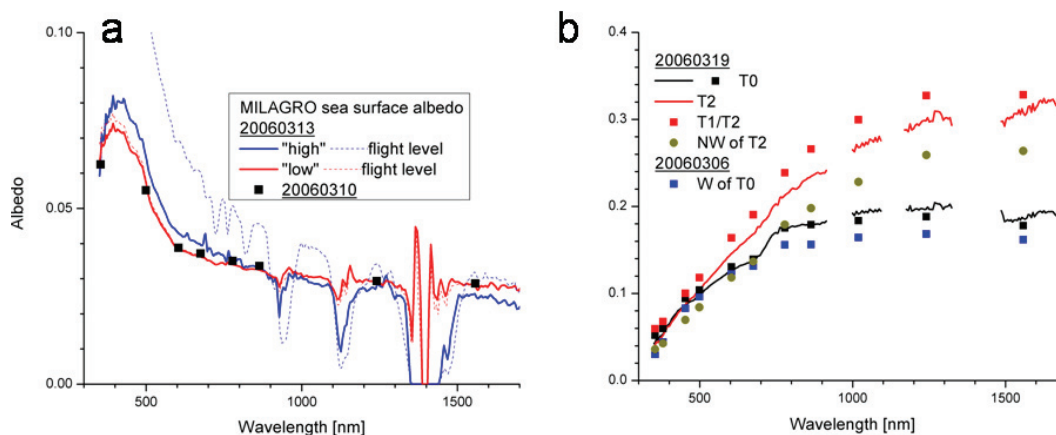


Fig. 9. Surface albedo retrievals over ocean **(a)** and land **(b)**. The dotted lines in (a) show the flight level albedo, the solid lines the spectra corrected for the effects of the atmosphere for a high-level leg (blue) and a low-level leg (red). The black dots stem from the new retrieval algorithm for 10 March. In (b), the lines show the atmospherically corrected results from Coddington et al. (2008); the symbols show the results from the new algorithm at nearby locations.

Title Page

Abstract

Introduction

Conclusions

References

Tables

Figures

◀

▶

◀

▶

Back

Close

Full Screen / Esc

Printer-friendly Version

Interactive Discussion

